An Investigation on the Effect of Drop Height, Roll Car Mass, and Radius of Gryration on Roll Car Motion

Group Thursday 1C

Patrick Carlson
Salvador Gomez
James Martin
Yara Mubarak
Colin Um

TABLE OF CONTENTS

1 ABSTRACT

Dropping a roll car from a top of the hill is a seemingly simple physics problem. However, many variables affect the motion of the roll car, such as friction, track deformation, slipping, aerodynamic drag, etc. Although a simplified physics model can be constructed to predict the roll car's dynamics, in some cases a more accurate model may be desired. Therefore, through experimental data, a model is developed that relates a roll car's drop height, mass, and radius of gyration to the position, velocity, acceleration, and number of complete passes over the center hill of a track.

2 INTRODUCTION

2.1 Objective

The objective of this experiment is to determine the effect of the roll car's drop height, mass, and radius of gyration on its position, velocity and acceleration, as well as the number of complete passes over the track. Using the data gathered, a physics model will be used to fit a partial differential equation (PDE) to the dynamics of the car, and then a numerical classification algorithm will be used to predict the coefficients of the PDE from the input variables.

2.2 Physics Model

Let h be the drop height of the roll car, v be the instantaneous velocity of the roll car, r_g be the radius of gyration of the roll car, ω be the angular velocity of the roll car, y be the instantaneous height of the roll car, and W_f be the work done by friction. By conservation of energy:

$$mgh = \frac{1}{2}mv^2 + \frac{1}{2}mr_g^2\omega^2 + mgy + W_f \tag{1}$$

If the roll car is not slipping, then $v = R\omega$, where R is the outer radius of the wheel of the roll car.

3 EXPERIMENTAL METHODS

3.1 Experimental Design Matrix

For the initial stages of the experiment, a $2x2x2$ matrix of experimental configurations of the variables h, m, and r_g is tested. Each configuration is tested 4 times so that the random error of the sensors can be determined. Table 1 lists the minimum and maximum values of each variable.

Table 1: Bounds on Variables

Variable	Minimum Value	Maximum value
h	23.3 cm	55.9 cm
m	508.2 g	1759.1 g
r_g	42.76 mm	45.59 mm

Ideally, for the $2x2x2$ experimental matrix, all combinations of the minimum and maximum values of the variables would be tested, for a total of 8 testing cases. However, in practice it is not possible to achieve all combinations of minimum and maximum variable values. For example, the radius of gyration and the mass cannot be independently varied because the mass distribution and shape of the roll cars' components are predetermined. Table 8 in the appendix lists the bounding area of the $2x2x2$ testing matrix and Table 9 lists the configurations tested in addition to the $2x2x2$ testing matrix. This data is also displayed graphically in Figure 1.

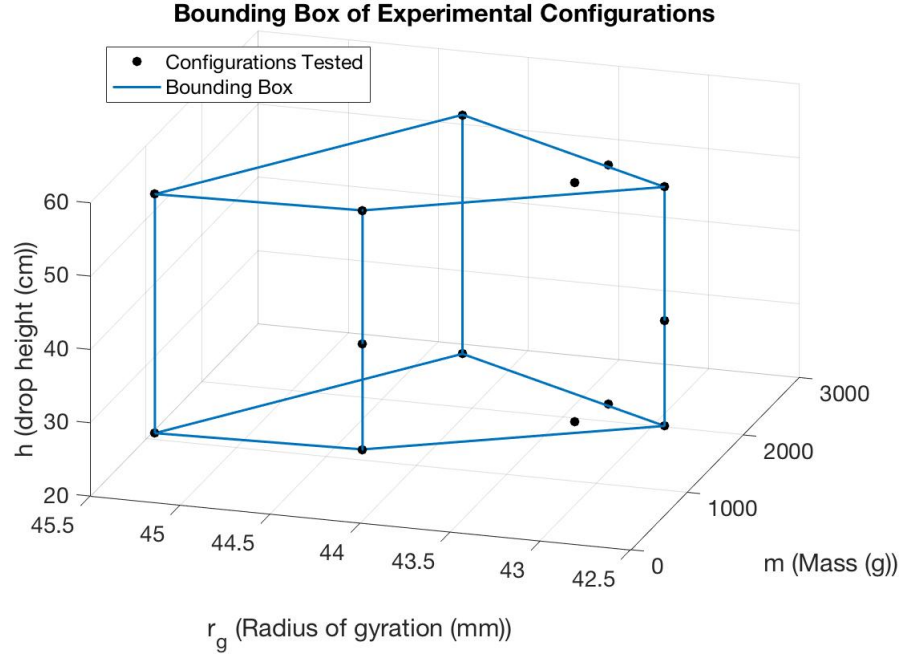**Bounding Box of Experimental Configurations**

Figure 1: Plot of experimental configurations tested. Points plotted only includes data from the initial 2x2x2 testing matrix.

3.2 Determining h, m, and r_g

Once the data for the $2x2x2$ testing matrix was collected, the variable that most affected the number of roll car passes was determined. Section 5.3 describes the subsequent steps for determining the final configurations that are tested.

To determine the height at which the roll car is released, h, the positions of the release points of the roll car are measured with rulers. m is determined by using a weigh scale. To determine the radius of gyration r_g, each component of the roll car is first replicated in SolidWorks and the moment of inertia I is calculated using the built-in moment of inertia calculator. By definition of the radius of gyration, $I = mr_g^2$ and therefore $r_g = \sqrt{\frac{I}{m}}$. To find the overall radius of gyration of a configuration obtained by placing together N components on the same axle, the following equation is used.

$$r_g = \sqrt{\frac{\sum_{i=1}^{N} m_i r_{g,i}^2}{\sum_{i=1}^{N} m_i}} \tag{2}$$

where m_i is the mass of component i and $r_{g,i}$ is the radius of gyration of component i.

3.3 Sensor List and Calibration

Along with measuring the position of the roll car, the physical properties of the roll car need to be measured to be able to predict the position of the roll car. In order to measure the position of the car, 16 phototransistors are placed along the length of the track. The phototransistor responds to the intensity of light on it. When the roll car passes over the phototransistor, the voltage increases as a result of the change in intensity. A threshold voltage is chosen to filter between the roll car passing over a phototransistor and background noise. A digital acquisition system (DAQ) is used to convert the phototransistor voltages into digital signals.

A ruler is used to measure the track and develop a model of the roll car's path to analyze the forces on the roll car. A caliper is used to measure the geometry of the roll car's components to then develop CAD

models of the various roll cars. A scale is used to measure the mass of the roll cars. Table 2 gives the list of the sensors used along with their respective resolutions.

Table 2: Sensor List

Sensor	Sensor Resolution
NI PCI-6251 DAQ	16 bit resolution
H21B1 Darlington Connected Phototransistor	Sampling Frequency of 250 Hz
Weigh Scale	0.1 g
Ruler	2 mm
Caliper	0.1 mm

Special care must be taken with the phototransistor because of the finite sampling frequency. A finite sampling frequency means that the phototransistor will not make an instantaneous measurement when the roll car is over the phototransistor. Because this introduces error in the time that the roll car passes over the phototransistor, that error is further propagated into the calculation of velocity and acceleration creating more noise in these measurements.

3.4 Converting Sensor Voltage to Position Data

The phototransistors are the sensors that translate the physical measurements of the position to a voltage which is converted to digital by a DAQ. If the sensor outputted a voltage of greater than a threshold voltage of 5 V, the roll car was said to be over the sensor. Due to the limitations of the phototransistors, such as finite sampling rate and finite time which the roll car passes over the sensor, the peaks in the voltage of a sensor is not localized to a point in time, but rather it is distributed along a time interval. Because of this, the time in which the roll car passes directly over the sensor is not well defined, and prone to noise. The average time at which the sensor detected the roll car was said to be the time at which the roll car was at the position of the sensor.

4 DIVISION OF LABOR AND PLANNING

Yara and Patrick are primarily responsible for developing and implementing the physics model. Salvador measured out the masses of the wheels and axles and used SolidWorks to compute the radius of gyration of the wheels and axles. Colin, Salvador, and James are in charge of processing raw data and writing the experimental methods, introduction, and results portion of the report. Everyone helped conduct the testing of the roll car.

On March 22, 2018, Salvador Gomez missed lab. To make up for his absence, he will, in addition to his normal duties described in the above paragraph, help Yara and Patrick develop the regression model and spend more time working on the Planning Report and Intermediate Report. On April 12, 2018, Yara Mubarak missed lab. To make up for her absence, she will, in addition to her normal duties, help Patrick Carlson with the code for the model. Yara will also spend more time with the intermediate report and help Salvador find configurations for the roll car to test.

Table 3: Proposed Schedule

Week #	Lab Date	In-lab Goal	Outside Lab Goal
1	03/15	Measure track, masses, and radii of gyration of roll car components.	Begin developing model. Start Planning Report.
2	03/22	Finish collecting data for $2x2x2$ matrix.	Determine most significant variable. Finish Planning Report.
3	04/05	Collect data for expanded experimental matrix.	Continue processing and analyzing data. Start Intermediate Report.
4	04/12	Collect data for expanded experimental testing matrix.	Continue processing and analyzing data. Finish Planning Report.
5	04/19	Collect data for expanded experimental testing matrix.	Finish model, prepare Presentation and start Final Report.
6	04/26	Conduct presentation and final configuration to test model.	Finish Final Report.

5   RESULTS AND DISCUSSION

5.1   Data Processing Procedure

The first step in the data processing procedure was to establish a threshold value for the sensor voltage. If the sensor voltage was above this threshold value V_t, then it would be assumed that the roll car was on top of the sensor. If the sensor voltage was below V_t, then it would be assumed that the roll car was not on top of the sensor. For the purposes of this experiment, $V_t = 5V$.

The average time t_{av} recorded by the sensor was taken to be the time at which the roll car passed over the sensor. For example, when the roll car passed over sensor 1, sensor 1 recorded multiple times for which the threshold value was exceeded. These times were then averaged to obtain a time t_{av} which was taken to be the time that the roll car passed the position of sensor 1.

5.2   Determining Velocity and Acceleration from Data

As outlined in Section 5.1, the position and time measurements for when the roll car passed over a sensor are determined by the sensor's position on the track and the average time for which the sensor's output voltage is above the threshold voltage. From this, there is a set of discrete data points for the position and time that the roll car passes the signal. Since the points are discrete and temporally spaced out, finding the velocity and acceleration of the roll car directly through a finite difference method will result in noise in the calculated velocities and accelerations. In order to smooth the position data out more, a third order polynomial is fit to blocks of four data points (the polynomial will pass exactly through these data points). That polynomial is then differentiated to output the velocity, and differentiated once again for the acceleration.

5.3   Model

Our Model is a two part model. The first part relies heavily on the dynamics of the roll car and the second is a standard regressive algorithm picked with the criteria of highest accuracy in mind. The pipeline being used looks as follows :
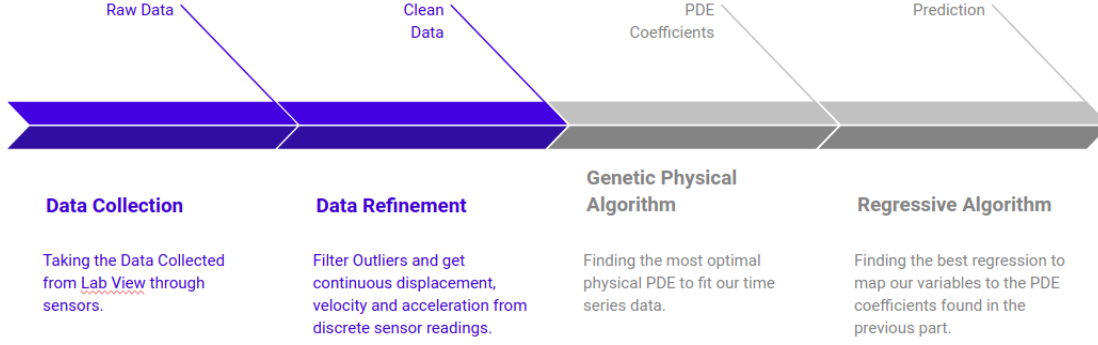
Figure 2: Project Coding Pipeline

The first two parts of the pipeline are described in sections 5.1 and 5.2, and this subsection will address the latter two.

5.3.1 Genetic Physical Algorithm

We are trying to determine the coefficients C_d, the drag coefficient, C_{RF} , coefficient of rolling friction, F_{IDK}, an unknown constant retarding force, μ_k, dynamic friction coefficient, μ_s , static friction and S_{init}, the initial drop position. It is given that $S(t_0) = S_{init}$, $\dot{S}(t_0) = 0$. $\theta(t_0) = 0$, $\dot{\theta}(t_0) = 0$. In addition, the curvature of the track $K(S)$, A_{CS} and the cross sectional area of the roll car can be determined by measurements. ρ_a, the density of air, can be determined by measuring the temperature and looking up values in the literature. It is assumed that the roll car dynamics are governed by the following equations:

If slipping is occurring (e.g. $abs(F_f) < \mu_s abs(F_n)$):

$$\ddot{S} = \frac{\vec{F}_r \cdot \vec{e}_t}{m(1 + \frac{r_g^2}{r_w^2})}$$

$$\ddot{\theta} = \frac{\ddot{S}}{r_w} \tag{3}$$

$$\vec{F}_n = mK\dot{S}^2 - \vec{F}_r \cdot \vec{e}_n$$

$$\vec{F}_f = m\ddot{S} - \vec{F}_r \cdot \vec{e}_t$$

Otherwise if there is no slip:

$$\ddot{S} = \frac{\vec{F}_r \cdot \vec{e}_t + \vec{F}_f}{m}$$

$$\ddot{\theta} = \frac{-\vec{F}_f r_w}{mr_g^2} \tag{4}$$

$$\vec{F}_n = mK\dot{S}^2 - \vec{F}_r \cdot \vec{e}_n$$

$$\vec{F}_f = \frac{\dot{S}}{|\dot{S}|}\mu_k \vec{F}_n$$

Finally for both cases:

$$\vec{F}_r = \frac{\dot{S}}{abs(\dot{S})}(F_{IDK} + C_{RF}F_n + 0.5A_{CS}\rho_a * |\dot{S}|^2 C_d) - mg\vec{E}_2 \tag{5}$$

In the genetic algorithm, the first step is to create an "initial population," which in this case is the values of the constants C_d, C_{RF}, F_{IDK}, μ_s, and S_{init}. Then, for each "member" of the population, the "error" of the

member is computed. In this case, the error is defined as the root mean square difference between the real roll car position data and the roll car position data created by assuming the value of the constants specified by the member of the population. In the next step, the next "generation" is created. In the genetic algorithm, the code creates "children," (e.g. new values of the constants C_d, C_{RF}, F_{IDK}, μ_s, and S_{init}) by taking the average of the members with the lowest root mean square error. In addition, a small amount of children are created by random combinations of members and a small amount of children are also created by making random changes in an existing member. The genetic algorithm continues making children until a certain tolerance is satisfied (e.g. the error of the simulation data generated from the constants is less than a specific number). A typical output from this genetic model is showing the model simulated motion against the data positions is shown in 3 and 4. These coefficients are then fed to the regressive algorithms.
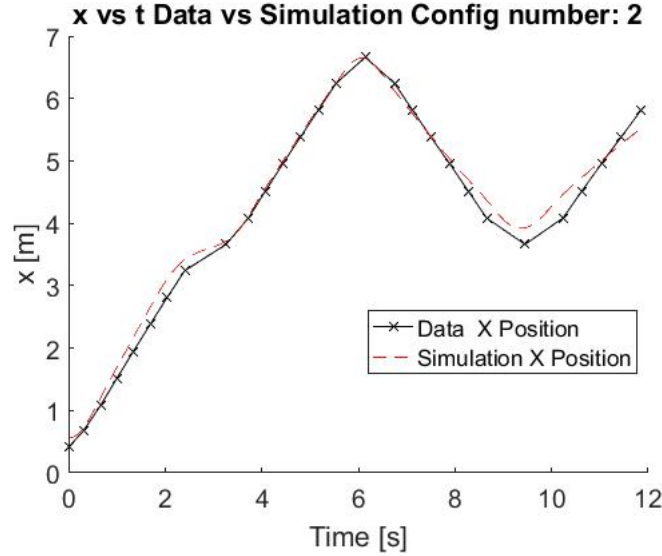

Figure 3: Comparison between model output and Data for x position vs time
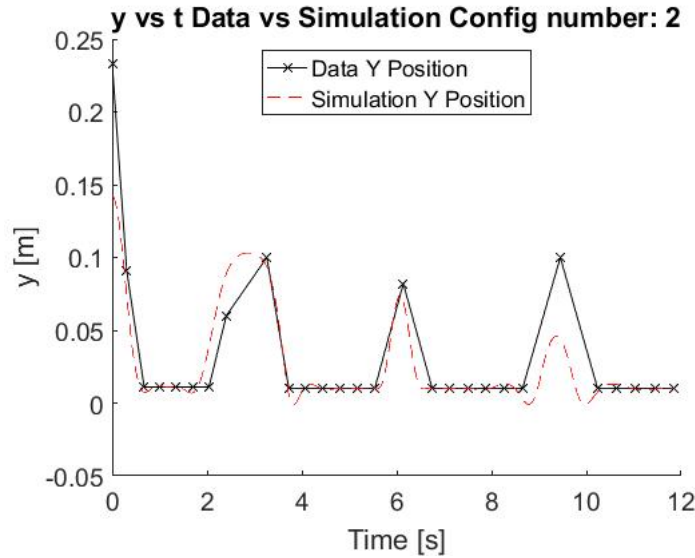

Figure 4: Comparison between model output and Data for y position vs time

Figures 3 and 4 show the output of the simulation for configuration 2. The simulation fits the actual data

well for most times and captures the overall behavior of the roll car by only taking one pass, as did the real car. However near the end, The model is draining energy away from the simulated car too fast, and the simulated cart does not get as high on the track as does the real car.

5.3.2 Regressive Algorithm

With the rising interest in machine learning, the library of available regressive algorithms (e.g. linear/nonlinear regression) in open source languages like python is growing exponentially. Therefore, with a good validation technique, the best algorithm can be picked for this application. From the genetic algorithm, the optimal coefficients for the kinematics PDE (equations 3-5) are given. Then, from the regressive algorithm, the effect of mass, radius of gyration and drop height on the coefficients (C_d, C_{RF}, F_{IDK}, μ_s, and S_{init}) can be determined. The goal of the second part of the model is to determine which regressive algorithm will best predict the effect of mass, radius of gyration, and drop height on these coefficients.

The feature matrix (e.g. the experimental data) used is comprised of the configurations of each of our trials. What is being predicted, usually termed the labels, are the coefficients of the PDE coefficients for each run. Leave-one-out cross validation is used to determine the accuracy of each regressive algorithm. This cross validation technique trains the algorithm on all the data set, but one point. That point is left to test on at the end. The mean squared error is then defined to be the average error of the algorithm. This technique is used because this model will be used to predict the kinematics of only one extra configuration at the end of lab.

5.4 Determination of Most Important Variable for Predicting Number of Passes
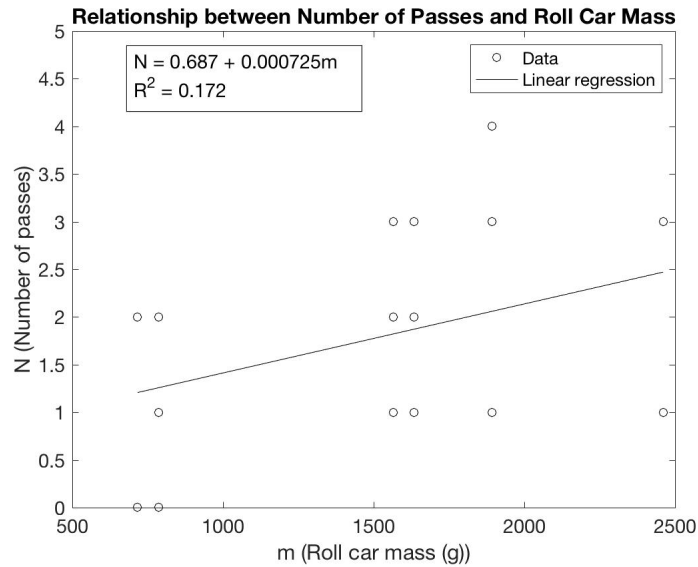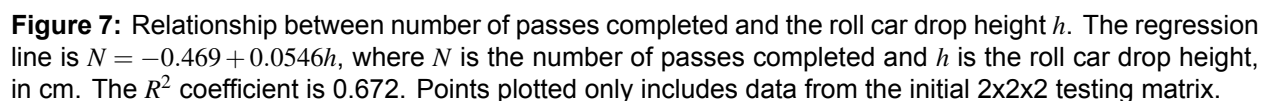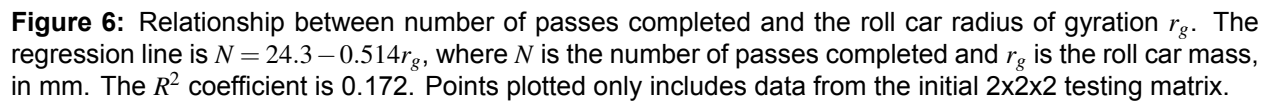

Figure 5: Relationship between number of passes completed and the roll car mass. The regression line is $N = 0.687 + 7.25 \times 10^{-4}m$, where N is the number of passes completed and m is the roll car mass, in g. The R^2 coefficient is 0.172. Points plotted only includes data from the initial 2x2x2 testing matrix.

Figure 6: Relationship between number of passes completed and the roll car radius of gyration r_g. The regression line is $N = 24.3 - 0.514 r_g$, where N is the number of passes completed and r_g is the roll car mass, in mm. The R^2 coefficient is 0.172. Points plotted only includes data from the initial 2x2x2 testing matrix.

Figure 7: Relationship between number of passes completed and the roll car drop height h. The regression line is $N = -0.469 + 0.0546 h$, where N is the number of passes completed and h is the roll car drop height, in cm. The R^2 coefficient is 0.672. Points plotted only includes data from the initial 2x2x2 testing matrix.

Figures 5,6,7 show that the number of passes N completed by the roll car most strongly depends on the drop height h of the roll car, since the R^2 coefficient between N and h (0.672) is significantly higher than the R^2 coefficients between N and r_g (0.172) and N and m (0.172). In Figure 7, as h increases, N increases, which makes sense since if the height is larger, it takes more passes for the frictional forces to dissipate the gravitational potential energy. The second most important parameter is the roll car mass. Figure 5 shows that as m increases, N increases. Figure 6 shows that as r_g increases, N decreases. This is because as the radius of gyration increases, it is more difficult for the ball to slip; thus additional rotational kinetic energy is

required to maintain the angular velocity of the roll car.

To maximize the predictive ability of our model, it is important to conduct tests at more drop heights than in the original 2x2x2 testing matrix. Therefore, in addition to the drop heights 1 and 10 tested in the original 2x2x2 testing matrix, drop heights $2, 4, 6, 8$ were tested. To isolate the effects of mass and radius of gyration on the roll car dynamics, two configurations with approximately the same mass but different radii of gyration were tested, and two configurations with the approximately the same radius of gyration but different masses were tested. The final testing matrix consists of a total of 38 configurations. For each of the drop heights 1 and 10 (Table Table 5), there were 10 mass and radius of gyration combinations tested. For the drop height 5, were 6 mass and radius of gyration combinations tested. For each of the drop heights $2, 4, 6, 8$, there were 3 mass and radius of gyration combinations tested. Table 4 lists all of the configurations that were tested, in order of increasing height. As of the intermediate report, all configurations that were planned to be tested have been tested. For the remaining week of testing, the goal is to conduct additional trials for the configurations that have been already tested.

5.5 *Effect of Mass, Radius of Gyration, and Drop Height on the Number of Passes Completed*
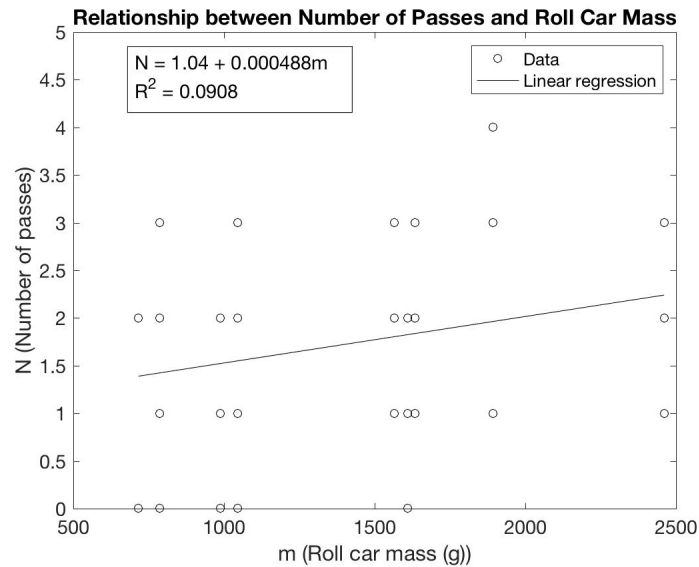

Figure 8: Relationship between number of passes completed and the roll car mass (includes all configurations). The regression line is $N = 1.04 + 4.88 \times 10^{-4} m$, where N is the number of passes completed and m is the roll car mass, in g. The R^2 coefficient is 0.0908. Note that this figure includes all configurations tested, while figure 5 only includes configurations in the 2x2x2 testing matrix.
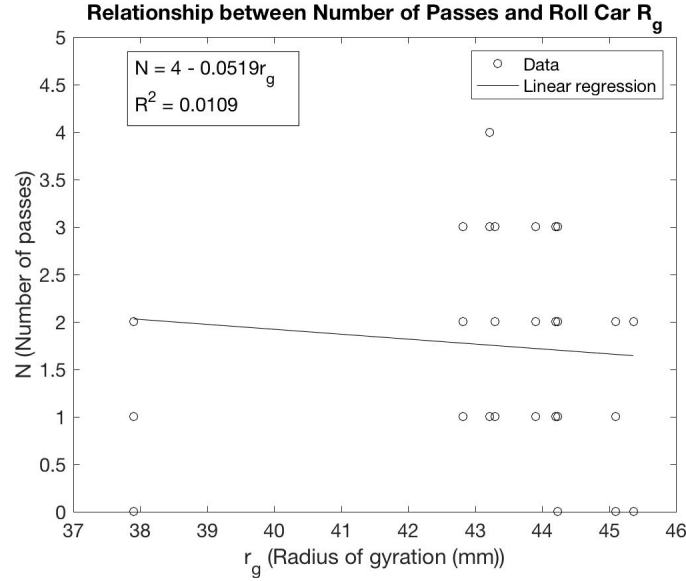
Figure 9: Relationship between number of passes completed and the roll car mass (includes all configurations). The regression line is $N = 4 - 5.19 \times 10^{-2}m$, where N is the number of passes completed and m is the roll car mass, in g. The R^2 coefficient is 0.0109. Note that this figure includes all configurations tested, while figure 6 only includes configurations in the 2x2x2 testing matrix.

Figures 8 and 9 show that the R^2 coefficient (0.0908) for the linear relationship between number of passes and roll car mass is higher than the R^2 coefficient (0.0109) for the linear relationship between number of passes and radius of gyration. Therefore, the mass more strongly affects the number of passes than the radius of gyration. The negative relationship indicates a smaller radius of gyration corresponds to more passes by the roll car. This is to be expected, since, in general, a lower radius of gyration corresponds to a lower moment of inertia, and thus a lower rotational kinetic energy. Therefore, less of the total energy of the roll car is lost in rotational kinetic energy and the roll car can undergo more passes. However, the effects of mass and radius of gyration on the number of passes of the roll car are coupled, so each individual variable has only a small correlation with the number of passes.
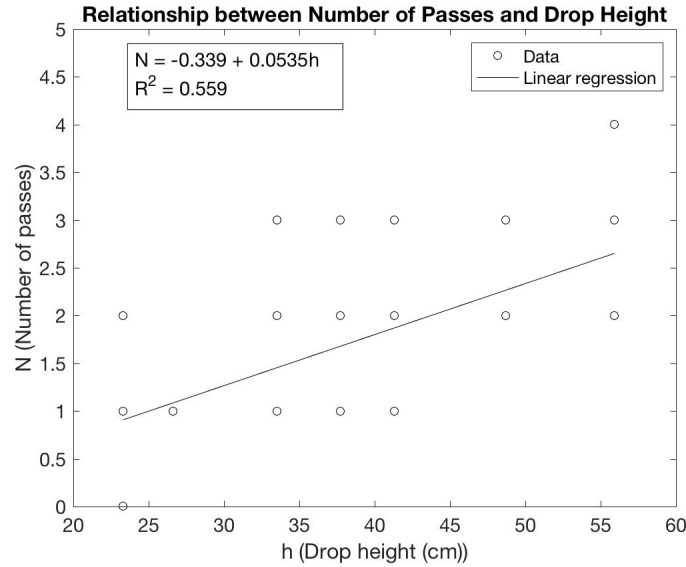
Figure 10: Relationship between number of passes completed and the roll car mass (includes all configurations). The regression line is $N = -0.339 + 5.35 \times 10^{-2}m$, where N is the number of passes completed and m is the roll car mass, in g. The R^2 coefficient is 0.559. Note that this figure includes all configurations tested, while figure 7 only includes configurations in the 2x2x2 testing matrix.

Figure 10 shows that, compared with the effect of mass and the effect of radius of gyration on the number of passes, the effect of drop height is more significant since the R^2 coefficient for number of passes and drop height (0.559) is much higher than the R^2 coefficient for number of passes and mass (0.0908) and the R^2 coefficient for number of passes and radius of gyration (0.0109). As the drop height increases, the number of passes increases accordingly. This is due to the increased potential energy that is associated with the increased drop height. Although one can argue that the mass also increases the initial potential energy, when one looks at the energy equation one finds that the energy equation has terms that are proportional to the mass. For instance, the kinetic energy, the potential energy, and even the dissipative force by friction will be to some extent proportional to the mass because of the normal force. Because of this, the effect of mass is to leading order negligible. The term which will affect the dynamics the most must be from the initial condition being the drop height.
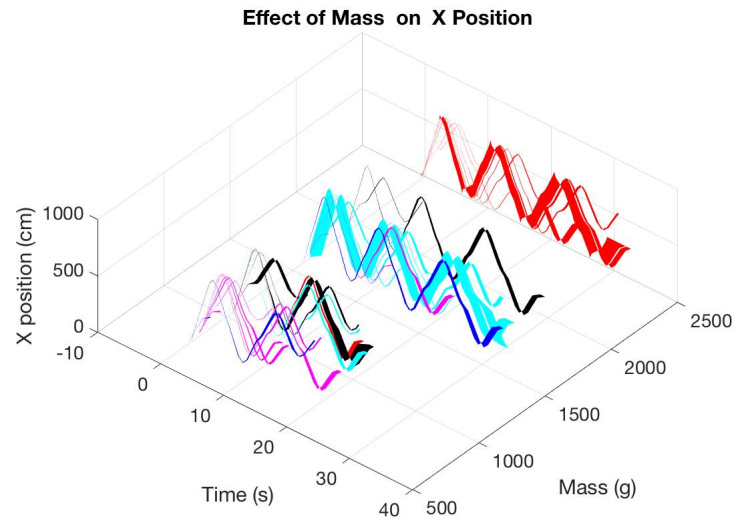
5.6   Effect of Mass on Kinematics

Effect of Mass on X Position

Figure 11: Effect of the Roll Car mass on the x position. The filled region represents the error in the x position. Full error analysis is in the Appendix.
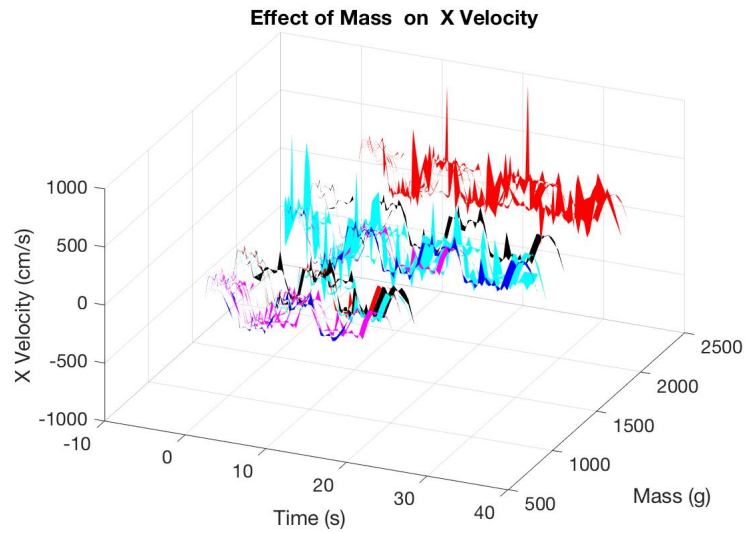
Effect of Mass on X Velocity

Figure 12: Effect of the Roll Car mass on the x velocity. The filled region represents the error in the x velocity. Full error analysis is in the Appendix.
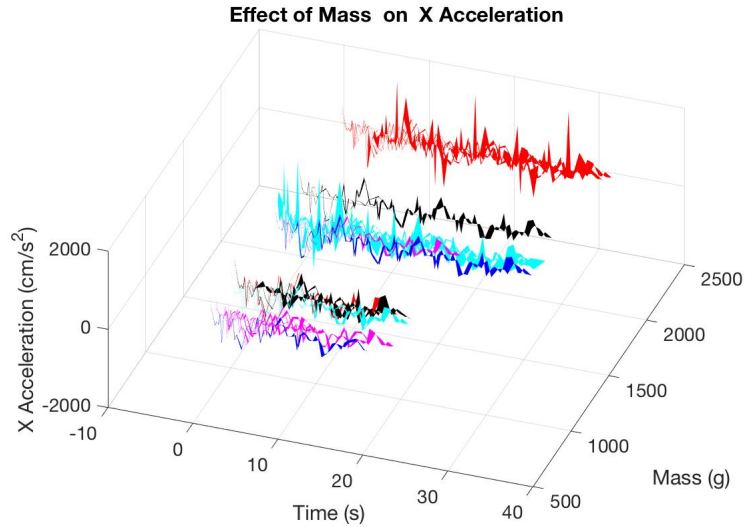
Effect of Mass on X Acceleration

Figure 13: Effect of the Roll Car mass on the x acceleration. The filled region represents the error in the x acceleration. Full error analysis is in the Appendix.

As can be seen from Figures 11, 12, and 13, the general shapes of the x position, x velocity, and x acceleration graphs are the same across all trials. The only major difference between the graphs is the the time domain of the graphs. There is a variation in how long it takes for the roll car to complete the runs (e.g. to fail to roll over the hill). The general trend that is evident in Figures 11, 12, and 13 is that larger masses general correspond to longer run times. This trend matches the results from 8, which shows that larger masses tend to correspond to a greater number of passes.

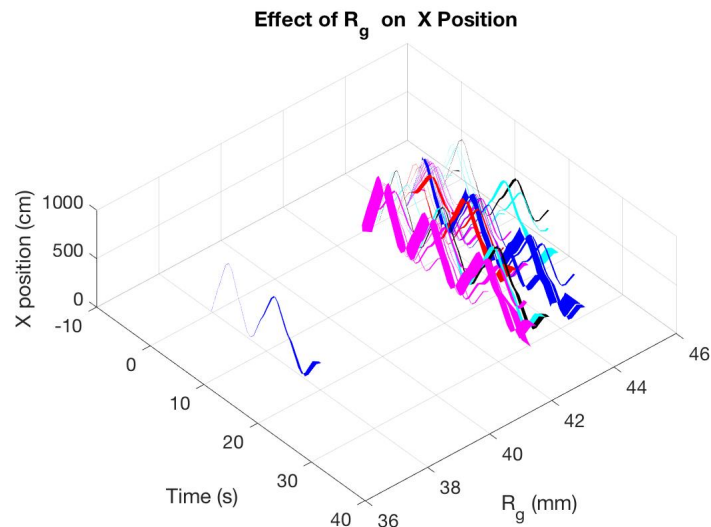*5.7   Effect of Radius of Gyration on Kinematics*

Effect of R$_g$ on X Position

Figure 14: Effect of the Roll Car radius of gyration on the x position. The filled region represents the error in the x position. Full error analysis is in the Appendix.
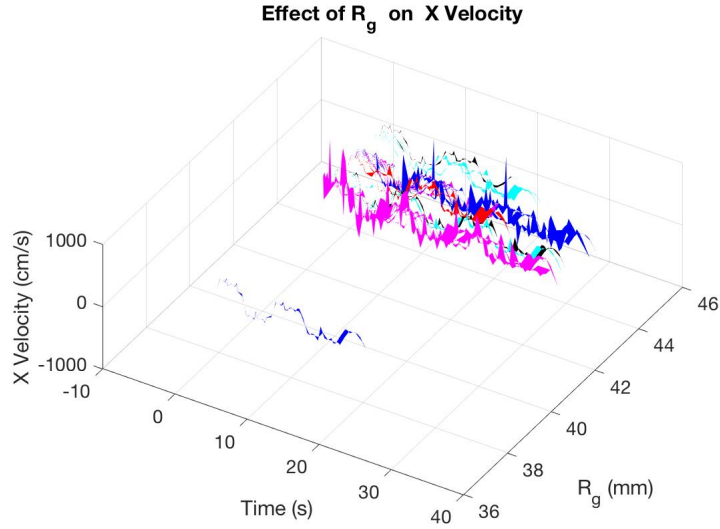
15

Effect of R$_g$ on X Velocity

Figure 15: Effect of the Roll Car radius of gyration on the x velocity. The filled region represents the error in the x velocity. Full error analysis is in the Appendix.

Effect of R$_g$ on X Acceleration

Figure 16: Effect of the Roll Car radius of gyration on the x acceleration. The filled region represents the error in the x acceleration. Full error analysis is in the Appendix.

As with the figures in section 5.6, the graphs of x position, velocity, and acceleration have the same general shape. As can be seen from Figures 14, 15, and 16 the lower radius of gyrations tend to correspond to longer roll car run times, but there are some exceptions, notably for radius of gyration 38 mm. This is because the mass and drop height, in addition to the radius of gyration, have an effect on the roll car kinematics.

5.8   Effect of Drop Height on Kinematics

Effect of Drop Height on X Position

Figure 17: Effect of the Roll Car height on the x position. The filled region represents the error in the x position. Full error analysis is in the Appendix.

Effect of Drop Height on X Velocity

Figure 18: Effect of the Roll Car drop height on the x velocity. The filled region represents the error in the x velocity. Full error analysis is in the Appendix.
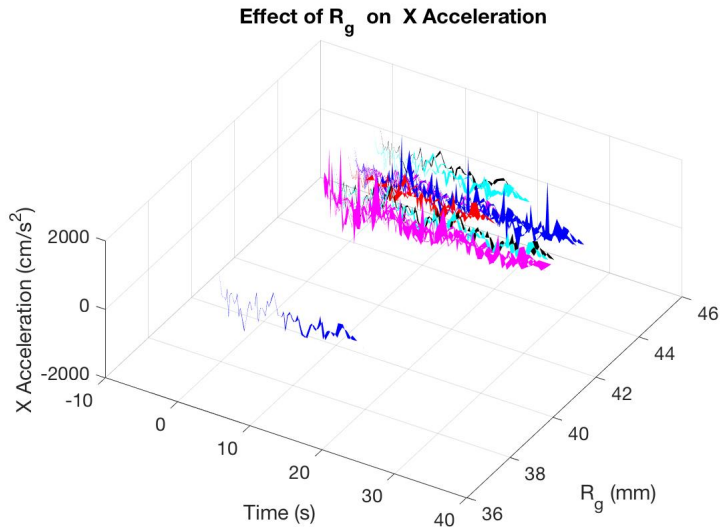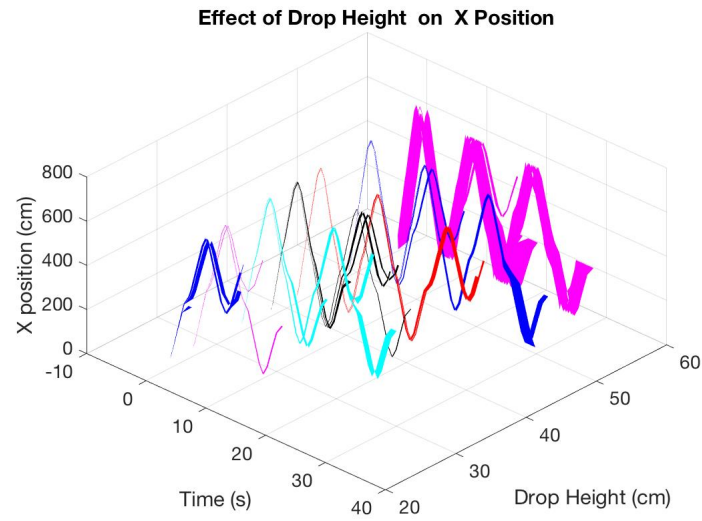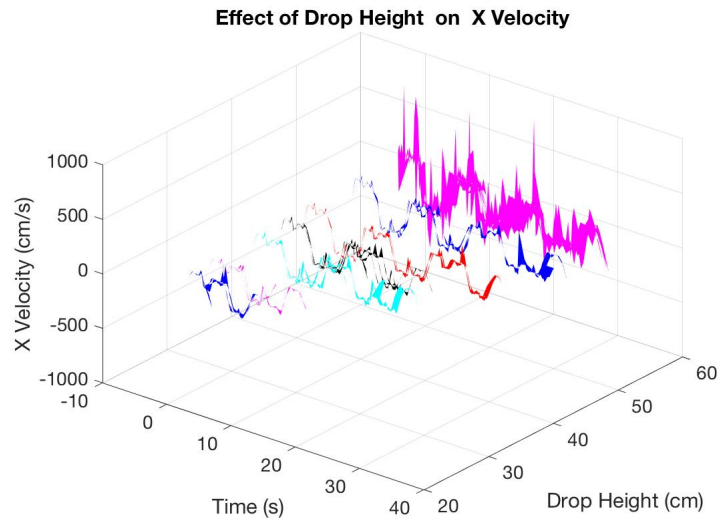
Effect of Drop Height on X Acceleration
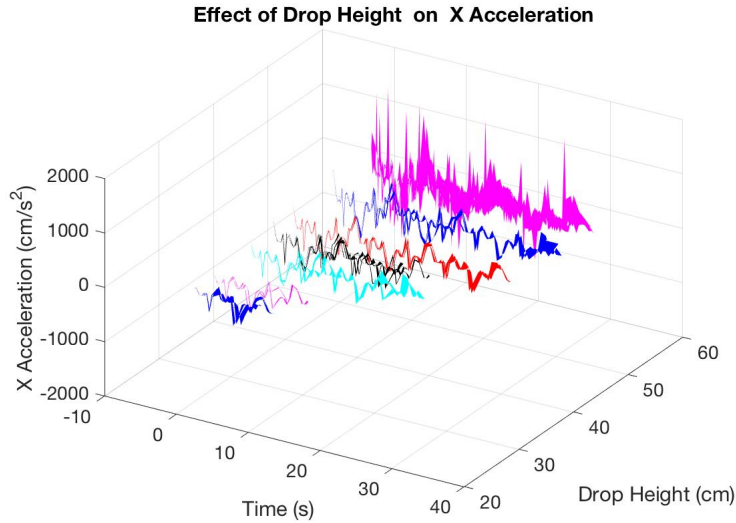
Figure 19: Effect of the Roll Car drop height on the x acceleration. The filled region represents the error in the x acceleration. Full error analysis is in the Appendix.

Unlike with the roll car mass and radius of gyration, there is a clear relationship between the roll car kinematics and the drop height. Figures 17, 18, and 19 show that for higher drop heights, the roll car run times are longer. In addition, for higher drop heights, the magnitudes of the x position, velocity and accelerations are larger. Physically, this makes sense, since a larger drop height means that the roll car will have a larger initial potential energy, at the bottom of the track, the roll car will have greater potential energy and thus greater velocity.

5.9   Comparison to Ideal Physics Model

Figure 20: Comparison of average energies of configurations with the ideal, frictionless physics model for different roll car masses.
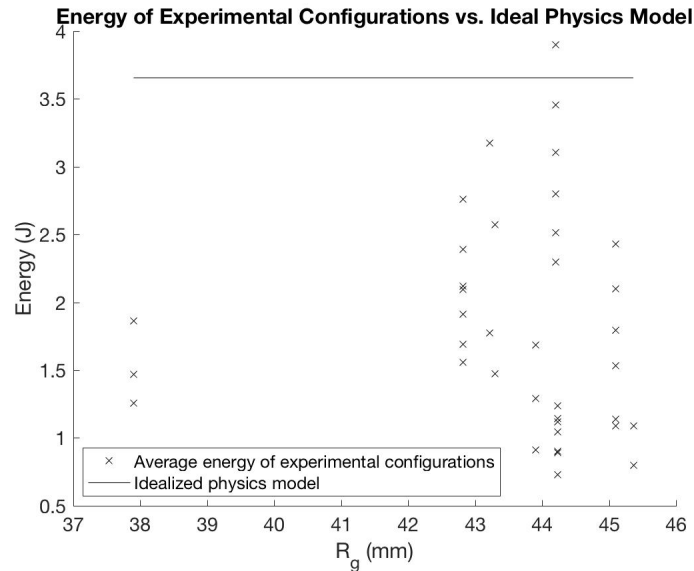
Figure 21: Comparison of average energies of configurations with the ideal, frictionless physics model for different roll car radius of gyration.
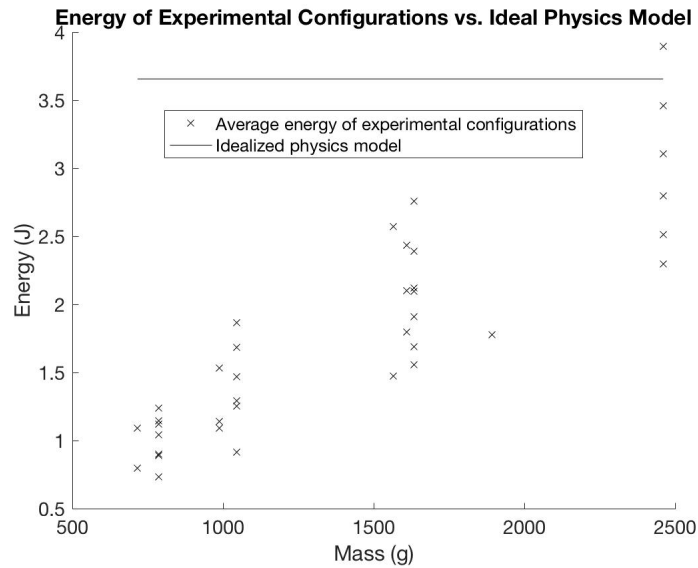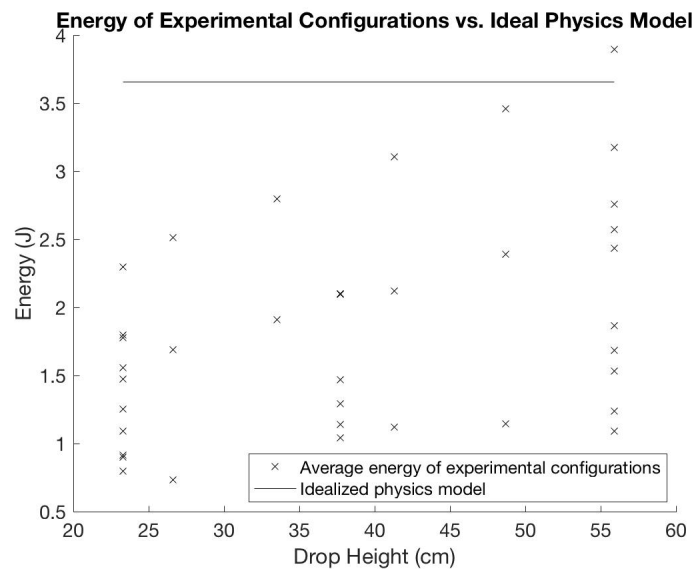

Figure 22: Comparison of average energies of configurations with the ideal, frictionless physics model for different roll car drop heights.

Figure 20 shows that as the mass increases, the average energy of the roll car throughout the test increases. This means that as the mass increases, the deviation of the ideal, frictionless physics model decreases and the rate of energy dissipation is slower. Figure 21 shows that there is no clear relation between the radius of gyration and the ability of the roll car to retain energy. Figure 22 shows that there is no clear relation between the drop height and the ability of the roll car to retain energy.

Note that in each of Figures 20, 21, and 22, there is one configuration that has a higher average energy than the average energy of the idealized physics model. This is because in this configuration, there were large errors in measuring the velocity, so the kinetic energy of this configuration was overestimated.

5.10 Summary of Number of Passes for Each Configuration

Table 4: Summary of Number of Passes for Each Configuration. The configurations are sorted in order of increasing height.

Configuration Number*	h** (cm)	m (g)	r_g (mm)	Number of Passes
7	23.3	716.5	45.3632	0
1	23.3	785.7	44.2322	0,1
30	23.3	988.5	45.0709	0,1
36	23.3	1044.4	43.8606	1
13	23.3	1564.7	43.2954	1,2
27	23.3	1610.6	45.0921	0
33	23.3	1046.4	37.8963	0,1
5	23.3	1633.9	42.8197	1,2
11	23.3	1892.1	43.2141	1
3	23.3	2460.7	44.1993	1
15	26.6	785.7	44.2322	1
23	26.6	1633.9	42.8197	1
19	26.6	2460.7	44.1993	1
16	33.5	785.7	44.2322	1
24	33.5	1633.9	42.8197	2,3
20	33.5	2460.7	44.1993	2
9	37.7	785.7	44.2322	1
31	37.7	988.5	45.0709	2
34	37.7	1046.4	37.8963	1,2
37	37.7	1044.4	43.8606	2,3
28	37.7	1610.6	45.0921	1,2
10	37.7	1633.9	42.8197	2
17	41.3	785.7	44.2322	1,2
25	41.3	1633.9	42.8197	3
21	41.3	2460.7	44.1993	3
18	48.7	785.7	44.2322	2,3
26	48.7	1633.9	42.8197	3
22	48.7	2460.7	44.1993	3
8	55.9	716.5	45.3632	2
2	55.9	785.7	44.2322	2
32	55.9	988.5	45.0709	2
38	55.5	1044.4	43.8606	2,3
35	55.9	1046.4	37.8963	2
29	55.9	1610.6	45.0921	2
6	55.9	1633.9	42.8197	3
14	55.9	1836.3	43.2954	3
12	55.9	1892.1	43.2141	3,4
4	55.9	2460.7	44.1993	3

* The configuration number refers to the assembly that corresponds to the configuration listed in Tables 8, 9, and 10.

** Note that the drop height listed here is the actual height in cm of the drop height location. This drop height is different from the drop height number. See Table 5 for a correspondence between drop heights and drop height number.

6 CONCLUSION

By performing a series of tests of the minimum and maximum values of the roll car drop height h, roll car mass m, and roll car radius of gyration r_g, it is determined that the number of passes N made by the roll car depended most strongly on h and most weakly depended on r_g. The ability of the roll car to retain energy throughout the tests most strongly depended on the roll car mass. With more configurations tested, the higher masses resulted in higher average energies of the roll car, meaning that for higher masses, the energy losses due to non-idealities such as friction were less significant compared to the total energy.

Because of the non-idealities and large number of variables, a genetic algorithm is set to fit coefficients based on a physics model that accounts for forces like drag and friction. The preliminary results from the genetic algorithm is able to predict the number of passes of a given configuration and to generate predictions of the x and y positions of the roll car, given the mass, radius of gyration, and drop height of the roll car.

7 List of Changes

- In Section 4, *Division of Labor and Planning*, we added what Yara Mubarak would do to make up for her absence in paragraph 2 of that section.

- In Section 5, we moved the Error Analysis to the Appendix. For the Error Analysis, we also added expressions for the uncertainty in velocity and acceleration.

- In Section 5.2, a discussion is included about how wee determine the acceleration and velocity from the position and time data.

- In Section 5.4 through 5.10 there is discussion about the effect of mass, drop height, and radius of gyration on the kinematics of the roll car.

- In Section 5, plots were added to demonstrate the effects of mass, radius of gyration, and drop height on the kinematics of the roll car.

- In Section 5.3 there is more discussion on the model.

References

[1] 2018, "Propagation of uncertainty". https://en.wikipedia.org/wiki/Propagation_of_uncertainty

8 APPENDIX

8.1 Error Analysis

As described in section 5.1, the phototransistors recorded the time taken for the roll car to pass over the sensor. The average t_{av} of these times is taken as the time at which the roll car passed over the sensor. If the standard deviations of these times were σ_t, then the 95% error u_t was taken to be:

$$u_t = t_{95\%, N-1} \times \frac{\sigma_t}{\sqrt{N}} \tag{6}$$

where N is the total number of trials conducted for a configuration (typically between 4 and 8), and $t_{95\%, N-1}$ is the 95% t-value with $N-1$ degrees of freedom. The error in the position measurements x and y was simply taken to be the resolution of the ruler (i.e. $u_x = u_y = 0.2\ cm$).

In general, the error in the time was more significant than the error in the position. The error in the position is on the order of 0.1 cm and is thus a negligible fraction of the length scale in the x and y directions of the track, which are on the order of 1000 cm and 10 cm, respectively. Therefore, in the following analysis on the error in the velocity and acceleration, the errors in the position u_x and u_y are neglected.

As described in section 5.2, the velocity and acceleration are determined by fitting a cubic polynomial to blocks of 4 data points. Suppose this polynomial is:

$$x(t) = a_0 + a_1 t + a_2 t^2 + a_3 t^3 \tag{7}$$

where a_0, a_1, a_2, and a_3 are constant coefficients, $x(t)$ is the x position (cm) as a function of time, and t is the time in s. Therefore, the x velocity $v_x(t)$ can be approximated as:

$$v_x(t) = a_1 t + 2a_2 t + 3a_3 t^2 \tag{8}$$

The x velocity $a_x(t)$ can be approximated as:

$$a_x(t) = 2a_2 + 6a_3 t \tag{9}$$

Since 4 data points are the minimum number needed to define a cubic polynomial, the coefficients of the cubic polynomial a_0, a_1, a_2, and a_3 will be exact. The only error is in the time t. By the Gaussian propagation of uncertainty:

$$u_{v_x} = \frac{dv_x}{dt} u_t \tag{10}$$

Noting that $\frac{dv_x}{dt} = a_x$,

$$u_{v_x} = a_x u_t \tag{11}$$

For the acceleration,

$$u_{a_x} = \frac{da_x}{dt} u_t \tag{12}$$

Note that $\frac{da_x}{dt}$ can be calculated by differentiating a_x.

8.2 Experimental Data

Table 5: Drop Heights The reference point (x=0 cm,y=0 cm) is located at the bottom right edge of the taller hill (see Figure 23). Note that y=0 cm is level with the bottom of the plastic strip of the track.

Drop Height Number	x coordinate (cm)	y coordinate (cm)
1	41.0	23.3
2	37.6	26.6
3	32.7	29.9
4	29.0	33.5
5	25.0	37.7
6	20.2	41.3
7	17.7	45.2
8	13.5	48.7
9	9.9	52.8
10	5.9	55.9

Table 6: Masses and Radii of Gyration of Roll Car Components

Component	Mass of component (g)	Radius of gyration (mm)
Aluminum center piece (thick)	412.3	46.3
Aluminum center piece (thin)	140.7	48.6
Plastic center piece	154.1	47.4
Steel center piece	980.9	46.9
Steel axle	76.6	29.6
Aluminum axle	20.8	29.6
Wheel (1 hole)	701.6	42.9
Wheel (16 holes)	277.5	45.0
Mega Nut	288.2	11.35
Mini Nut	12	.71
Thin Nut	8.3	.72

Table 7: Locations of sensors. The reference point (x=0 cm,y=0 cm) is located at the bottom right edge of the taller hill (see Figure 23). Note that y=0 cm is level with the bottom of the plastic strip of the track.

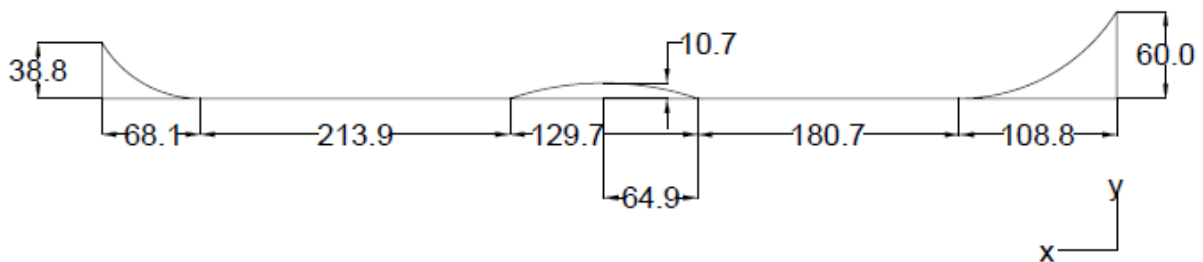| Sensor #	x coordinate (cm)	y coordinate (cm)
1	67.2	9.1
2	109.1	1.1
3	151.3	1.1
4	194.5	1.1
5	238.0	1.1
6	281.0	1.1
7	324.0	6.0
8	366.1	10.0
9	408.4	1.0
10	451.5	1.0
11	495.9	1.0
12	538.1	1.0
13	581.3	1.0
14	524.2	1.0
15	666.1	8.2
16	698.1	37.0

Figure 23: Track schematic.

Table 8: Bounding Configurations of $2x2x2$ Test Matrix

Configuration	Assembly	h (cm)	m (g)	r_g (mm)
1	Plastic Center Piece + Steel Axle + 16 Hole Wheel	23.3	785.7	44.2322
2	Plastic Center Piece + Steel Axle + 16 Hole Wheel	55.9	785.7	44.2322
3	Steel Center Piece + Steel Axle + 1 Hole Wheel	23.3	2460.7	44.1993
4	Steel Center Piece + Steel Axle + 1 Hole Wheel	55.9	2460.7	44.1993
5	Plastic Center Piece + Steel Axle + 1 Hole Wheel	23.3	1633.9	42.8197
6	Plastic Center Piece + Steel Axle + 1 Hole Wheel	55.9	1633.9	42.8197
7	Thin Aluminum Center Piece + Aluminum Axle + 16 Hole Wheel	23.3	716.5	45.3632
8	Thin Aluminum Center Piece + Aluminum Axle + 16 Hole Wheel	55.5	716.5	45.3632

Table 9: Additional Configurations

Configuration	Assembly	h (cm)	m (g)	r_g (mm)
9	Plastic Center Piece + Steel Axle + 16 Hole Wheel	37.7	785.7	44.2322
10	Plastic Center Piece + Steel Axle + 1 Hole Wheel	37.7	1633.9	42.8197
11	Thick Aluminum Center Piece + Steel Axle + 1 Hole Wheel	23.3	1892.1	43.2141
12	Thick Aluminum Center Piece + Steel Axle + 1 Hole Wheel	55.9	1892.1	43.2141
13	Thin Aluminum Center Piece + Aluminum Axle + 1 Hole Wheel	23.3	1564.7	43.2954
14	Thin Aluminum Center Piece + Aluminum Axle + 1 Hole Wheel	55.9	1836.3	43.2954
15	Plastic Center Piece + Steel Axle + 16 Hole Wheel	26.6	785.7	44.2322
16	Plastic Center Piece + Steel Axle + 16 Hole Wheel	33.5	785.7	44.2322
17	Plastic Center Piece + Steel Axle + 16 Hole Wheel	41.3	785.7	44.2322
18	Plastic Center Piece + Steel Axle + 16 Hole Wheel	48.7	785.7	44.2322
19	Steel Center Piece + Steel Axle + 1 Hole Wheel	26.6	2460.7	44.1993
20	Steel Center Piece + Steel Axle + 1 Hole Wheel	33.5	2460.7	44.1993
21	Steel Center Piece + Steel Axle + 1 Hole Wheel	41.3	2460.7	44.1993
22	Steel Center Piece + Steel Axle + 1 Hole Wheel	48.7	2460.7	44.1993
23	Plastic Center Piece + Steel Axle + 1 Hole Wheel	26.6	1633.9	42.8197
24	Plastic Center Piece + Steel Axle + 1 Hole Wheel	33.5	1633.9	42.8197
25	Plastic Center Piece + Steel Axle + 1 Hole Wheel	41.3	1633.9	42.8197
26	Plastic Center Piece + Steel Axle + 1 Hole Wheel	48.7	1633.9	42.8197
27	Steel Center Piece + Steel Axle + 1 Hole Wheel	23.3	1610.6	45.0921
28	Steel Center Piece + Steel Axle + 1 Hole Wheel	37.7	1610.6	45.0921
29	Steel Center Piece + Steel Axle + 1 Hole Wheel	55.9	1610.6	45.0921
30	Thick Aluminum Center Piece + Aluminum Axle + 1 Hole Wheel	23.3	988.5	45.0709
31	Thick Aluminum Center Piece + Aluminum Axle + 1 Hole Wheel	37.7	988.5	45.0709
32	Thick Aluminum Center Piece + Aluminum Axle + 1 Hole Wheel	55.9	988.5	45.0709
33	Plastic Center Piece + Aluminum Axel + 16 Hole Wheel + Mega Nut + Mini Nut + Mini Nut + Thin Nut	23.3	1046.4	37.8963

Table 10: Additional Configurations (continued)

Configuration	Assembly	h (cm)	m (g)	r_g (mm)
34	Plastic Center Piece + Aluminum Axel + 16 Hole Wheel + Mega Nut + Mini Nut + Mini Nut + Thin Nut	37.7	1046.4	37.8963
35	Plastic Center Piece + Aluminum Axel + 16 Hole Wheel + Mega Nut + Mini Nut + Mini Nut + Thin Nut	55.9	1046.4	37.8963
36	Thick Aluminum Center Piece + Steel Axel + 16 Hole Wheel	23.3	1044.4	43.8606
37	Thick Aluminum Center Piece + Steel Axel + 16 Hole Wheel	37.7	1044.4	43.8606
38	Thick Aluminum Center Piece + Steel Axel + 16 Hole Wheel	55.5	1044.4	43.8606